Development of aqueous protein/polysaccharide mixture-based inks for 3D printing towards food applications

Chi Zhang [1], Chang-Sheng Wang [1], Daniel Therriault [2] * and Marie-Claude Heuzey [1]**

[1] *Department of Chemical Engineering, Research Center for High Performance Polymer and Composite Systems (CREPEC) , Polytechnique Montréal, 2900 Boulevard Edouard Montpetit, Montréal, Québec H3T 1J4, Canada*

[2] *Laboratory for Multiscale Mechanics (LM2), Department of Mechanical Engineering, Research Center for High Performance Polymer and Composite Systems (CREPEC), Polytechnique Montréal, 2900 Boulevard Edouard Montpetit, Montréal, Québec H3T 1J4, Canada*

∗ Corresponding author: daniel.therriault@polymtl.ca (D. Therriault)

∗∗ Corresponding author: marie-claude.heuzey@polymtl.ca (M-C. Heuzey)

ABSTRACT

Three-dimensional (3D) food printing is a promising technique as it allows to create elaborated food constructs or customized food for elderly people and other sensitive population (i.e. children, pregnant women or athletes). The structural and textual properties of food constructs depend strongly on the ingredients used and the shape produced. Two important biological macromolecular components, namely protein and polysaccharides, are the most important in terms of nutritional content. In this work, we developed a water-based protein/polysaccharide food ink from a mixture of gelatin B (GB) and xanthan gum (XG) for 3D printing. A 40-layer 3D scaffold with defined features was successfully printed at room temperature using an aqueous mixture of 3 wt% GB and 10 wt% XG. Adding 37.5 mM calcium ions (Ca^{2+}) or lowering the storage temperature to 4 °C improved the rheological properties of the ink, which endowed the scaffold with higher shape fidelity right after printing and good shape retention for at least 96 h. Texture profile results revealed that the infill percentage of the scaffold is critical to textural properties of the scaffold, highlighting the advantage of 3D printing in tuning sensory food perception.

Keywords: 3D food printing; Gelatin; Xanthan gum; calcium salt; rheological properties; textural profile results

1. Introduction

Three-dimensional (3D) food printing is an emerging manufacturing technology using the additive principle through computer-controlled layer-by-layer deposition of materials (Liu, Zhang, Bhandari, & Yang, 2018). It enables the production of customized food designs and creative food flavors with personalized nutrition according to individual health conditions (Lille, Nurmela, Nordlund, Metsä-Kortelainen, & Sozer, 2018; Sun, Zhou, Huang, Fuh, & Hong, 2015). Additionally, 3D food printing technology is a convenient production process (H. W. Kim, Bae, & Park, 2017). It allows to fabricate complex food design with precise temperature controlled during the printing process (Sun, Zhou, Yan, Huang, & Lin, 2018) and with relatively less material loss (Vancauwenberghe, et al., 2017). Therefore, it has the potential to replace some of the more cumbersome processes of traditional food production methods (Chen, et al., 2019; H. W. Kim, et al., 2017).

The first reported 3D printer goes back to 2007 at Cornell University where the researchers developed the "Fab@Home" model (Gross, Erkal, Lockwood, Chen, & Spence, 2014). Since then, researchers have developed different printing techniques, such as extrusion-based printing, selective laser sintering and inkjet printing etc.(Wegrzyn, Golding, & Archer, 2012). Direct-ink writing (DIW) is a 3D printing technique employing a computer-controlled translation stage, which moves an ink-deposition micro-nozzle, to generate materials with controlled design and composition. It is an adaptable approach which offers flexibility requirement for soft materials, such as colloidal suspensions, fugitive ink and hydrogels. So far, several food inks including chocolate (Lanaro, et al., 2017), pasta (Godoi, Prakash, & Bhandari, 2016), mushroom (Keerthana, Anukiruthika, Moses, & Anandharamakrishnan, 2020), cheese (Le Tohic, et al., 2018) and fish gel (Lin Wang, Zhang, Bhandari, & Yang, 2018) have been successfully printed using the DIW technique. Different mechanisms have been employed to facilitate shape retention during post extrusion, including solvent evaporation, gelation, temperature control and UV polymerization. However, there is still a lack of fundamental knowledge on 3D printing of essential constituents of food (H. W. Kim, et al., 2017; Liu, et al., 2018; Sun, Peng, et al., 2015).

Proteins and polysaccharides are two important biological macromolecules in food systems, which perform complementary nutritional, structural and textural functions (C. S. Wang, Virgilio, Wood-Adams, & Heuzey, 2017; X.-Y. Wang, Wang, & Heuzey, 2015). Attractive (biopolymers with

opposite charges) and repulsive interactions (biopolymers with same or no charge) can occur depending on the environmental pH and ionic strength (Zeeb, Thongkaew, & Weiss, 2014). Electrostatic forces and hydrogen bonding are usually the dominant interactions between the two components, while other weak interactions should also be considered such as van der Waals forces and hydrophobic interactions (McClements, 2006). Different functional attributes can be provided by these interactions, such as the ability to thicken solutions, form gels or emulsions (Tolstoguzov, 1995).

Gelatin, a linear protein, is obtained by either acid (type A) or alkaline (type B) hydrolysis of the parent protein collagen, which is derived from animal skin and/or bones (Williams & Phillips, 2003). It has a helix-to-coil transition temperature, below which the random coils assemble into triple helices, resulting in gelation via forming a 3D network (Joly-Duhamel, Hellio, Ajdari, & Djabourov, 2002). Xanthan gum (XG) is an anionic food-grade polysaccharide produced by aerobic fermentation, which is composed of a β-(1-4)-D-glucose main chain and a trisaccharide branch (D-glucose, D-mannose and D-gluconate) as side chains (Pelletier, Viebke, Meadows, & Williams, 2001). The XG molecules undergo a thermal-reversible coil-helix transition in solution, and the transition temperature can be shifted to higher temperatures by the addition of electrolytes (Song, Kim, & Chang, 2006) or proteins (C.-S. Wang, Virgilio, Wood-Adams, & Heuzey, 2018). XG is widely used in food engineering owing to its shear-thinning properties as well as the resistance against heat, acids, bases, salts and even enzymes (C.-S. Wang, Natale, Virgilio, & Heuzey, 2016; C.-S. Wang, Virgilio, Carreau, & Heuzey, 2021). Moreover, required food properties can be easily adjusted by XG addition, such as viscosity, texture appearance, etc. (Kumar & Saini, 2021; Salehi, 2020). Although XG is a non-gelling polysaccharide, it can form a gel in the presence of trivalent ions or when mixed with other polysaccharides, or even proteins (Bertrand & Turgeon, 2007; Le & Turgeon, 2013; C.-S. Wang, et al., 2021; C.-S. Wang, et al., 2018; C. S. Wang, et al., 2017).

Several food inks have been developed so far. For example, gel formed by low methoxylated pectin (an anionic polysaccharide) has been used to print edible objects with DIW (Vancauwenberghe, et al., 2017). The printed 3D structure can be greatly stabilized with the addition of $CaCl_2$ during and after printing, due to ion bridging effects. The 3D printability of a mixture of gelatin and kappa-carrageenan was investigated by Warner et al.(Warner, Norton, & Mills, 2019). It was found that

the addition of kappa-carrageenan enabled better control of the printing process compared to pure gelatin and they attribute it to the increase of the gelling temperature.

Synergistic gelation properties have been previously reported for gelatin B (GB) with XG in aqueous solution at a pH around the isoelectric point of GB (pI~5.3) (C.-S. Wang, et al., 2016). In addition, the gel preparation process does not involve thermal, enzyme or any other denaturing treatment, which is favorable for protecting micronutrients in food. It provides a promising way to fabricate group-specific food. However, up to now, there is no specific study in the literature on 3D printing of GB/XG mixed gels with careful parameter control and detailed structure analysis.

In this work, we aim to shed light on the 3D printing of a protein/polysaccharide mixed gel system for food application. 3D printing of a mixture of GB and XG based on the DIW method is presented and analyzed in terms of the interactions between GB and XG. The effects of Ca^{2+} addition and storage temperature after printing on shape retention, gel strength and textural properties are investigated in order to clarify the printed object quality.

2. Materials and methods

2.1. Materials

Gelatin (type B, G6650, bloom index ~225, molecular weight: 20-25 kDa, pI = 4.7-5.3) and $CaCl_2 \bullet 2H_2O$ were purchased from Sigma-Aldrich Canada. XG (KELTROL RD, food-grade quality, molecular weight: ~10^3 kDa) was supplied by CP Kelco U.S. All other reagents and chemicals were of analytical grade and used without further purification.

2.2. Food ink preparation

GB solutions (3 wt%) were prepared by allowing the GB to swell in Milli-Q water (18.2 Ω) for 15-20 min, followed by gentle magnetic stirring at 40 °C for 15 min. The solutions were used on the same day. 10 wt% XG dry powder was then added to the GB solution. The GB/XG mixed solution was mechanically stirred at a speed of 600-700 rpm for at least 12 h at 40 °C to ensure complete dissolution. The final pH of prepared solution was 5.8. For comparison purposes, a neat XG solution of 10 wt% concentration was also prepared. Ca^{2+} was added to the GB/XG aqueous mixture at concentrations that varied from 0, 12.5, 37.5, 62.5 to 75 mM, within the recommended

intake by the Institute of Medicine (IOM) (Ross, et al., 2011). The pH did not change with Ca^{2+} addition. The ink was then centrifuged (5000 rpm, 1 h) at room temperature (22 ℃) to eliminate air bubbles.

2.3.3D printing process and 3D scaffold fabrication

The food ink was inserted into a syringe (3 mL, Nordson EFD) linked with a cylindrical micronozzle (exit inner diameter D = 200 μm, capillary length L = 12.7 mm, Nordson EFD). Then the loaded syringes were fixed to a high-pressure adaptor (HP-7x Nordson EFD), which was installed on a computer assisted 3-axis positioning stage (I&J2200-4, I&J Fisnar Inc.). The 40-layer 3D scaffold was printed by depositing filaments in a layer-by-layer manner with the GB/XG food ink, as well as with different concentrations of Ca^{2+} solution. All scaffolds were printed at a speed of 7 mm/s and under appropriate applied pressures at room temperature (22 ± 1 ℃). The speed of 7 mm/s was chosen based on preliminary experiments as a compromise between shape fidelity and printing time. Specific applied pressures are reported in the legend of **Figure S1**.

2.4.Rheological measurements

In the low shear rate region (0.01-10 s^{-1}), steady-shear measurements of GB/XG aqueous mixtures were performed using a rough surface parallel plate flow geometry with 25 mm diameter with a stress-controlled rheometer (MCR-502, Anton Paar, Graz, Austria). The gap between the plates was 1 mm. A rough surface was chosen to prevent wall slip. Mineral oil was used to cover the edge of the sample in the parallel plate flow geometry to prevent water evaporation. The measurements were carried out at room temperature (22 ℃).

In the high shear rate region, the process-related viscosity was calculated by capillary flow analysis (CFA) (Bruneaux, Therriault, & Heuzey, 2008; Guo, Heuzey, & Therriault, 2014). Different food inks were loaded into the syringe (3 mL, Nordson EFD). A 60 mm filament was extruded onto a glass substrate through a micronozzle (exit inner diameter D = 200 μm, capillary length L = 12.7 mm, Nordson EFD) at a speed of 0.5 mm/s for 120 s with each food ink. The different pressures were set under a range between 70 and 900 kPa. The weight of each extruded filaments was then measured with a high-precision balance (GH-202. A&D Engineering) at room temperature, which was used to calculate the process-related viscosity according to the method reported by Bruneaux et al.(Bruneaux, et al., 2008).

The effects of Ca^{2+} and storage temperature after printing on the dynamic viscoelastic properties of the food inks were also investigated using the same geometry. Linear viscoelastic (LVE) regime was determined by strain sweeps in the range from 0.01 % to 100 % at angular frequency = 1 rad/s. Frequency sweeps were performed over a range of 0.1 to 10 rad/s within the identified LVE regime (strain = 0.2-5%). The storage modulus (*G'*) and loss modulus (*G''*) were recorded using Rheocompass software (Anton Paar).

For samples stored at 4 ℃, the lower plate was pre-cooled down at 4 ℃ using the temperature-controlled Peltier system before the test. All the rheological experiments were performed three times.

2.5.Morphological characterization

Optical images of 2D and 3D structures were captured using an optical microscope (BX-61, Olympus) and a digital camera (EOS TRBRL T4I, Canon). The images were then analyzed with Image Pro Plus 6.0 (Media Cybernetics).

2.6.Determination of dimensional stability of 3D-printed structures

The printed dimensional stability obtained using the different food ink formulations was evaluated by directly following the thickness variation of the as-printed 3D scaffolds up to 96 h. The images of the samples were recorded 0, 24 and 96 h after printing, respectively. The thickness of the samples was measured using a caliper. All samples were put in petri dishes and then stored under a hood in order to maintain constant room temperature and humidity, or in a refrigerator at 4 ℃.

2.7.Compression tests for textural profile analysis

Mach-1^{TM} Micromechanical tester (Biomomentum Inc.) was used for a double-cycle compression tests to obtain load-time curves. A 25 mm diameter cylindrical probe was used to compress the printed 40-layers 3D scaffolds (18 mm × 18 mm) composed of GB/XG food inks with different Ca^{2+} contents and different infill levels (**Figure 1a**). The main test setting parameters are listed in **Table 1**. Triplicate measurements of samples were carried out. **Figure 1b** shows how the various properties of the textural profile test are measured and calculated. More explanations on the various properties measured are given in the Results and discussion section.

Table 1. Parameters used for the compression tests

Setting parameters	Value	Unit
Contact force	1	g
Contact speed	0.1	mm/s
Test speed	0.5	mm/s
Withdrawal speed	0.5	mm/s
Compression distance	2	mm

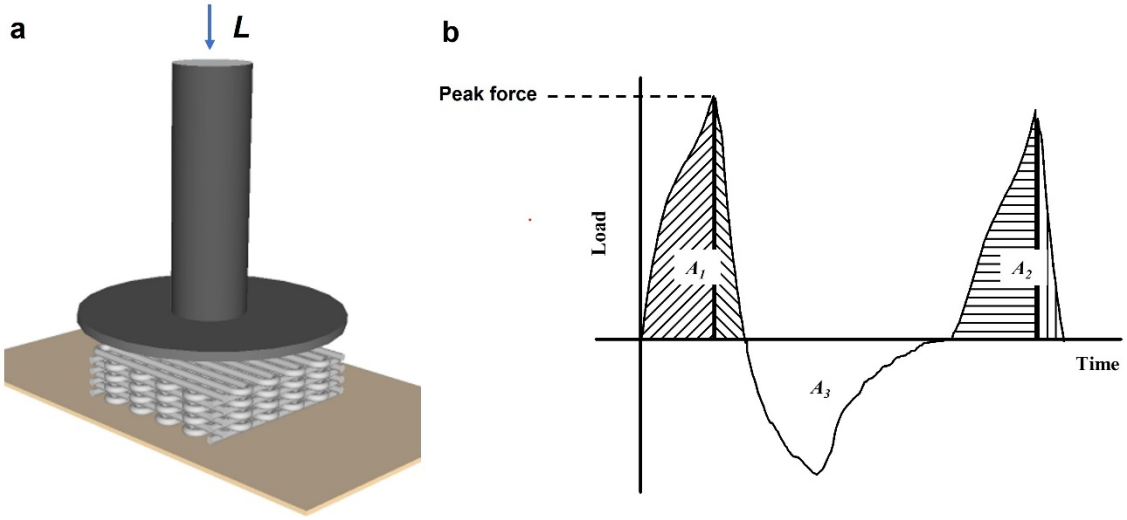

198

199 **Figure 1**. (a) Schematic representation of the compression test using the Mach-1^{TM}
200 Micromechanical tester (b) Textural profile diagram for gels. (Hardness: Peak Force;
201 Cohesiveness: A_2/A_1; Adhesiveness: A_3; Gumminess: Hardness × Cohesiveness.)

202 **2.8.Statistical analysis**

203 Triplicate tests have been performed for all the tests mentioned above. The mean of the results ±
204 standard deviation (SD) was used to present the data and analyzed by SPSS software (SPSS 20.0,
205 IBM, Chicago, IL, USA). Significant differences ($p < 0.05$) between mean values of samples were
206 determined using Duncan's Multiple Range test.

207

208 **3. Results and discussion**

209 ***3.1.3D printed structures***

210 **Figure 2a** and **2b** show the 3D printing process using the food ink based on GB/XG aqueous
211 mixture and the scaffold model used, respectively. The effect of salt addition is observable when
212 XG concentration is higher than 0.3% (Chang, Im, Prasidhi, & Cho, 2015; de Moura & Moreno,

2019; Zatz & Knapp, 1984). Considering a gel which can flow under applied pressure and maintain its structures after deposition, 10 wt% XG has been selected. Hence, a formulation of ink with 3 wt% GB and 10 wt% XG aqueous mixture has been obtained after carefully adjusting the composition. It allowed printing a scaffold with accurate features (**Figure 2c**). In comparison, the scaffold printed with a neat 10 wt% XG aqueous solution does not retain its structure after deposition, exhibiting a poor self-supporting behavior (**Figure S1a**). Hence, it is clear that the addition of GB imparts improved printability to the food ink. The addition of Ca^{2+} enhances the shape retention of the scaffold printed by the food ink of GB/XG mixtures, as shown by the sharper edges (**Figure 2c** and **2d)**.

The top-view printability (*Pr*) (Equation 1) defined by Ouyang et al. (Ouyang, Yao, Zhao, & Sun, 2016) is used to quantitatively describe and compare the gelation condition and shape fidelity of the food inks. The *Pr* is calculated based on the circularity (*C*) (Equation 2) estimated by the perimeter *L* and pore area *A* (schematically shown in **Figure 2e**). When the *Pr* value is equal to 1, the interconnected channels of the filaments show a square shape, indicating an ideal gelation. Larger *Pr* value presents a greater gelation degree. Otherwise ($Pr < 1$), a lower gelation degree is noted. **Figure 2e** and **2f** show the top-view images of the as-printed GB/XG scaffold with 0 and 37.5 mM of Ca^{2+} along with their *Pr* values. These values show that the printability of both food inks is within the proper range, while the one with Ca^{2+} addition is slightly closer to 1, indicative of better printability with this content of Ca^{2+} in the GB/XG food ink.

$$Pr = \frac{\pi}{4} \cdot \frac{1}{C} = \frac{L^2}{16A} \quad (1)$$

$$C = \frac{4\pi A}{L^2} \quad (2)$$

However, 62.5 mM Ca^{2+} addition (**Figure S1d**) causes irregular extrusion with structure defects. The poor structure quality is probably due to an over-gelation of the printed filament. Among the tested Ca^{2+} concentrations, the scaffold with 37.5 mM Ca^{2+} shows the best appearance (**Figure 2d and Figure S1c**).

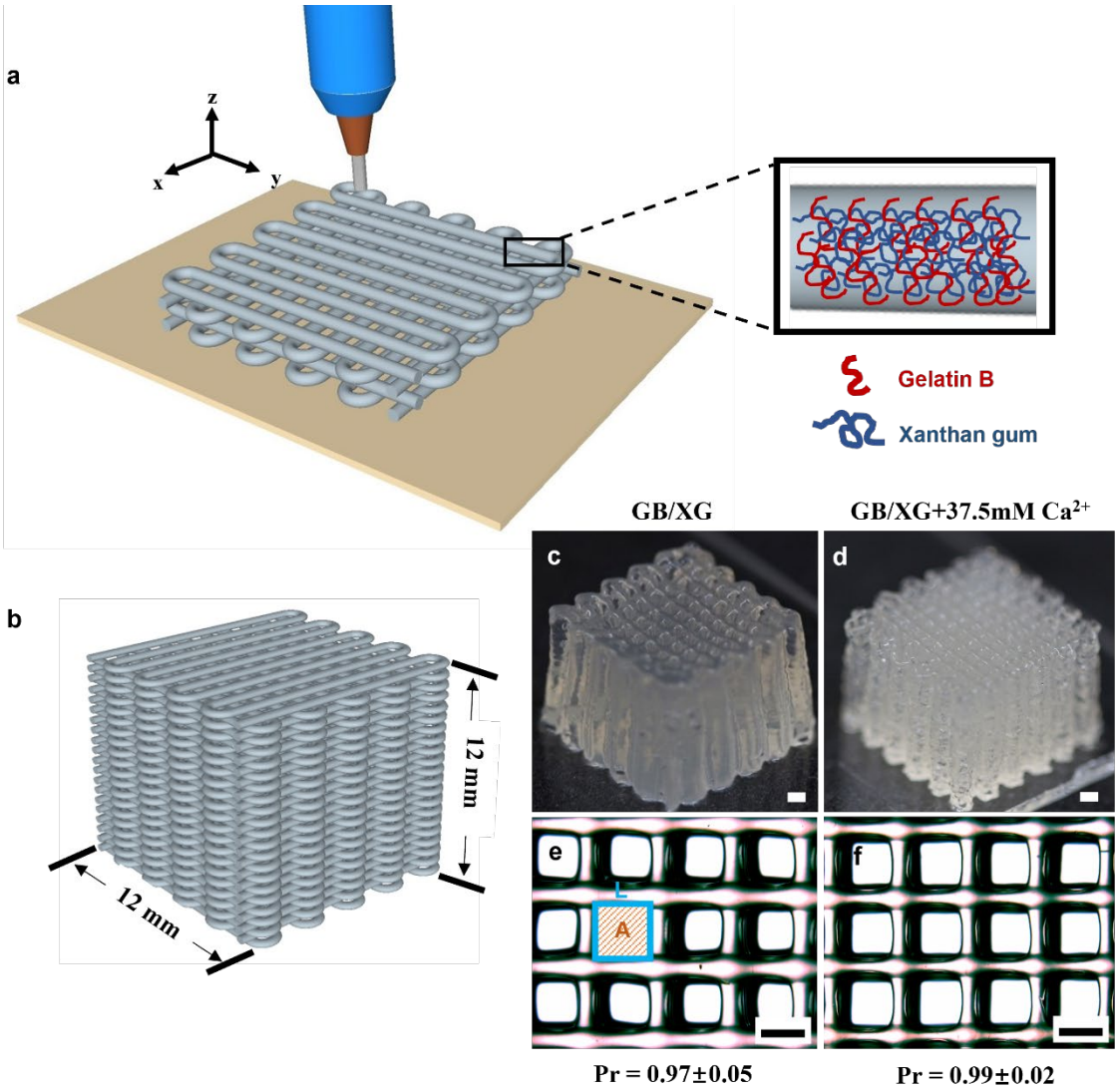

239

240 **Figure 2**. (a) Schematic representation of the 3D printing process with the food ink; (b) Model of
241 the 40-layers 3D scaffold, (c) As-printed 40-layers GB/XG scaffold and (d) GB/XG + 37.5 mM
242 Ca^{2+} scaffold using 200 μm nozzle; (e) Representative optical top-view image of a GB/XG scaffold
243 and (f) GB/XG + 37.5 mM Ca^{2+} scaffold. All the photos and images were taken at room
244 temperature right after printing. Scale bar is 1 mm. The printing time for a 12 mm × 12 mm scaffold
245 is around 10 min.

246 ***3.2.Rheological properties of food inks***

247 The rheological properties of the GB/XG ink are of critical importance since they are directly
248 related to the extrusion process and ensure successful flow through the micronozzle and good post-
249 deposition properties.

Figure 3 shows the shear viscosity of neat XG and the 3 wt GB/10 wt% XG aqueous mixture with different Ca^{2+} concentrations. The solid symbols in the low-to-moderate shear rate region (~ 0.01-10 s^{-1}) represent the steady-shear viscosity of the food inks measured by rheometer at room temperature. The open symbols in the higher shear rate region (> 10 s^{-1}) show the process-related apparent viscosity of the food inks as a function of the process-related shear rate. These results were calculated from capillary flow analysis (CFA) (Guo, et al., 2014) data obtained using a nozzle diameter of 200 μm when extruding the material at room temperature. All food inks demonstrated a shear-thinning behavior, which is favorable for the printing process. The viscosity decreases significantly with increasing shear rate, with a relatively low power-law index (*n*) (**Table 2**), typical of soft solids such as XG (J.A. Carmona, 2017). The data measured by rotational rheometer (RR) is generally coherent with the data calculated from CFA. However, as seen in **Table 2**, *n* values calculated from CFA are relatively higher than the results measured using the rheometer. The decreased shear rate dependency indicates that the structure of the food inks is already rather oriented or stretched in capillary flow (Ansari, Rashid, Waghmare, & Nobes, 2020; Drabek, Zatloukal, & Martyn, 2018).

Compared with XG alone, the GB/XG food ink shows higher viscosity, which might be due to their synergistic interactions, which benefits the gelation of hydrocolloids. The electrostatic repulsions between GB and XG enhance the local concentration of XG. In addition, XG also interacts with the negative patches on GB by electrostatic attractions (C.-S. Wang, et al., 2016). As shown in **Table S1**, the viscosity increased by approximately 46 % for food ink with GB addition at 1 s^{-1}. On the other hand, an increase in the viscosity of the GB/XG food ink was observed in the presence of Ca^{2+}, which is probably due to the bridging effect of Ca^{2+} with XG molecules (Freitas, Cortez-Vega, Pizato, Prentice-Hernández, & Borges, 2013; Mohammed, Haque, Richardson, & Morris, 2007; Patel, Maji, Moorthy, & Maiti, 2020) and/or negative patches on GB. With the increase of Ca^{2+} concentration, the viscosity at 1 s^{-1} of different food inks ranged from 158 ± 30 to 720 ± 91 Pa.s (**Table S1**). A maximum viscosity is obtained when Ca^{2+} concentration is 62.5 mM. Further increasing the Ca^{2+} concentration to 75 mM does not lead a significant change in the viscosity. Therefore, an appropriate improvement in viscosity benefits the extruding ability of food ink and thus the printability.

Table 2. Power-law index of different food inks within two specific shear rate regimes (two methods)

Food ink type	Power-law index (n)	
	Low to moderate shear rate (RR)	High shear rate (CFA)
Pure 10 wt% XG gel	0.18±0.02	0.27±0.07
GB/XG gel with no salt	0.16±0.03	0.25±0.07
GB/XG gel with 12.5 mM Ca^{2+}	0.14±0.03	0.24±0.04
GB/XG gel with 37.5 mM Ca^{2+}	0.12±0.03	0.22±0.02
GB/XG gel with 62.5 mM Ca^{2+}	0.12±0.02	0.21±0.03
GB/XG gel with 75 mM Ca^{2+}	0.12±0.02	0.21±0.03

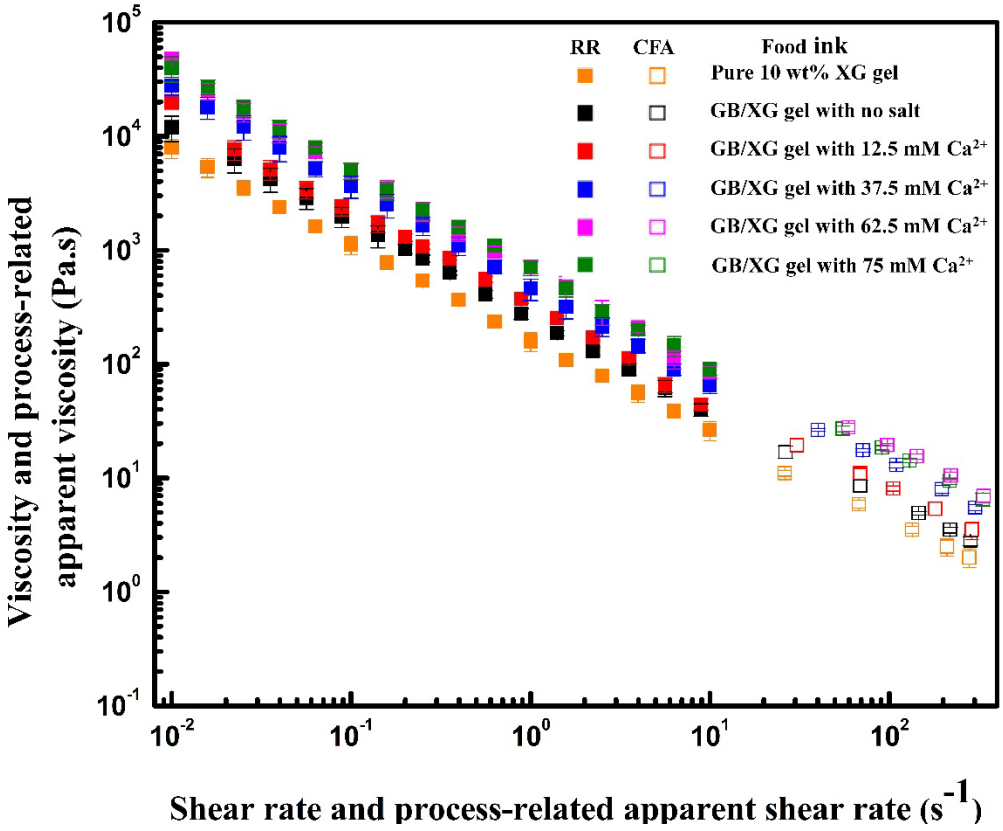

Figure 3. Viscosity as a function of shear rate for XG and GB/XG food ink with different Ca^{2+} concentrations at room temperature (22 ℃) (solid symbols: data measured using a parallel plate flow geometry in steady shear (RR); open symbols: data obtained by capillary flow analysis (CFA).

Linear viscoelastic properties of neat XG solution and GB/XG food ink with 0-37.5 mM Ca^{2+} addition were also measured to infer the post-deposition quality, and the results are shown in **Figure 4**. For all food inks, the linear viscoelastic regime is identified in-between a strain

amplitude of 0.2-5% (**Figure 4a**). The storage modulus *G'* dominates the loss modulus in all the investigated strain and frequency ranges (**Figure 4a and 4b**). In addition, *G'* of GB/XG food ink without salt is almost 1.5 times larger than *G'* of neat 10 wt% XG. Adding Ca^{2+} to the ink leads to an increase of *G'*, possibly due to the bridging effects of Ca^{2+} (Freitas, et al., 2013; Mohammed, et al., 2007; Patel, et al., 2020), which enhances the gel strength of the gel formulation and also allows the corresponding ink to retain a high shape fidelity after deposition (**Figure 2f**). Comparing Ca^{2+} concentration ranging from 0 to 37.5 mM, *G'* gradually increased from 452 ± 26 to 1720 ± 68 Pa (380%) (**Table S2**). Similar observations of gel properties enhancement have been found for the gelatin-transglutaminase (TG) system (Du, et al., 2021). The increases were almost 2 times in *G'* at 1 rad/s and viscosity at 1 s^{-1} at low very content of transglutaminase (2 mg/mL) due to strong chemical crosslinking between gelatin and TG as opposed to physical crosslinking between gelatin and calcium ions. Regarding the power-law parameter *a* on frequency dependency of *G'* (**Table S3**), it decreased when lowering the temperature, which resulted in a strengthening in gel structure. The decrease in frequency dependence indicated a more solid-like behavior when decreasing the temperature. Lowering the temperature to 4 °C favors the intra- and intermolecular hydrogen bonding formation (Zhang, Wang, Wang, Han, & You, 2020), which boosts the formation of stiffer structures, such triple helical structure of GB (Bello, Kim, Kim, Park, & Lee, 2020) and double helical structure of XG (Lei Wang, Xiang, Li, Zhang, & Bai, 2021). This results in a higher *G'* and enhances the gel strength of the food ink. For example, the *G'* of the GB/XG food ink with 12.5 mM Ca^{2+} addition at frequency of 1 rad/s is 2040 ± 97 Pa at 4 °C, which is about twice higher than the *G'* measured at room temperature (**Table S2**).

Table S2 also summarizes the tan δ of different food inks at an angular frequency of 1 rad/s. The presence of GB in XG, the addition of Ca^{2+} and lower temperature resulted in lower tan δ values, which were in a range from 0.08 to 0.15. Those gels can be qualified as weak gels (Rao, 2014), which benefited for the printing process.

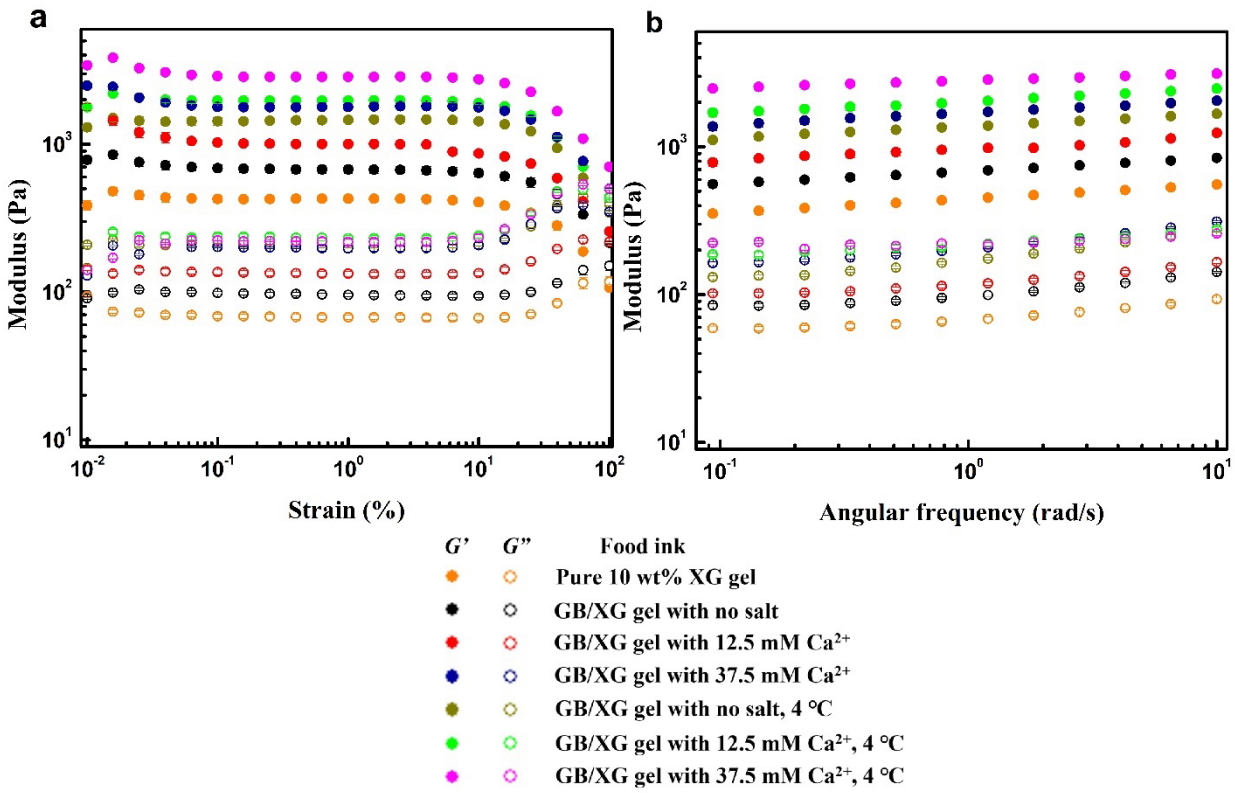

313

314 **Figure 4**. Storage modulus G' (solid symbols) and loss modulus G'' (open symbols) for XG gel
315 alone and GB/XG mixed gels with different Ca^{2+} addition at room temperature (RT) and 4 °C: (a)
316 as functions of strain amplitude (%) at $\omega = 1$ rad/s (b) as functions of angular frequency at
317 strain = 1%.

318 ***3.3 Dimensional stability of 3D-printed structures***

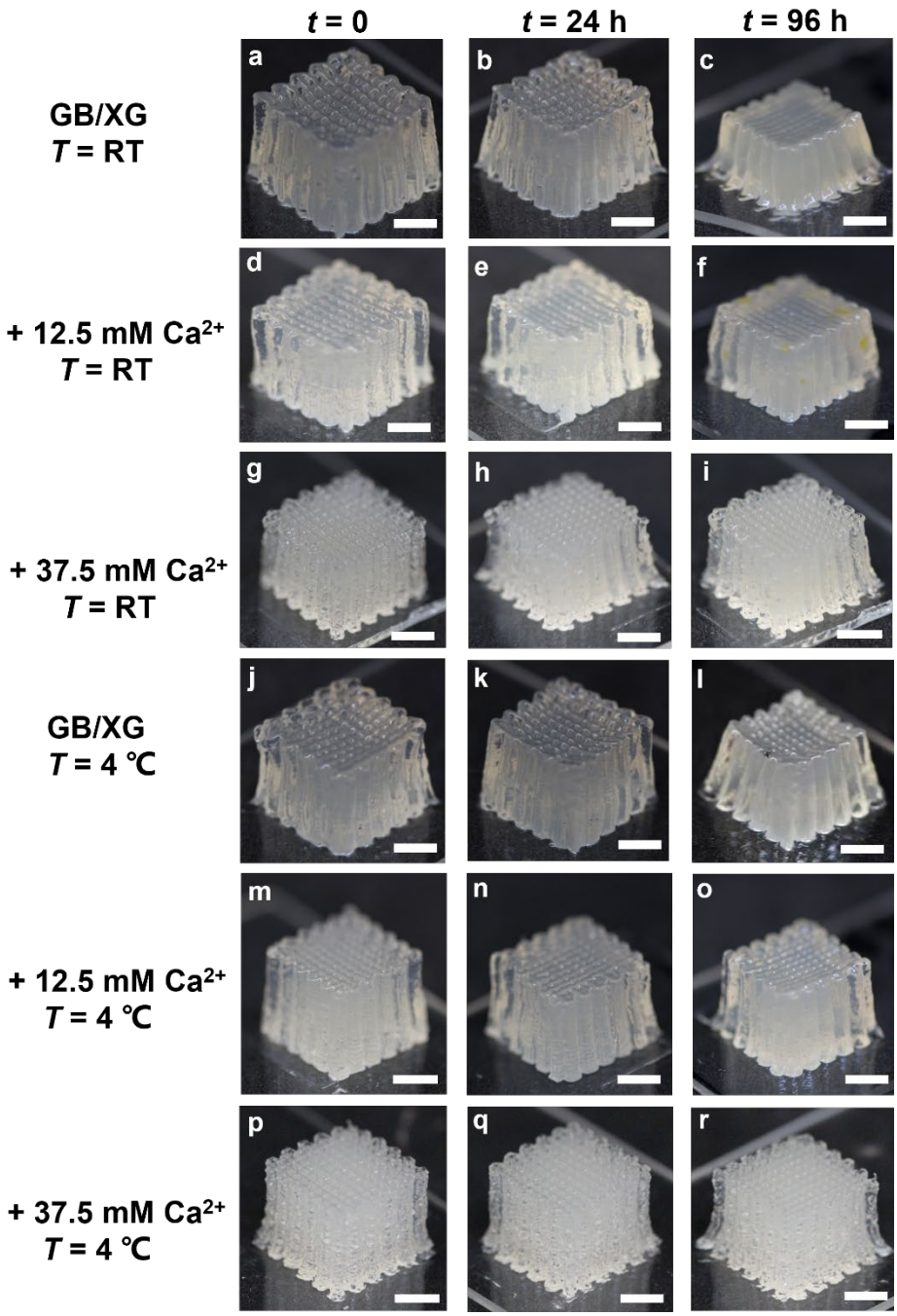
t = 0
t = 24 h
t = 96 h
GB/XG
T = RT
+ 12.5 mM Ca2+
T = RT
+ 37.5 mM Ca2+
T = RT
GB/XG
T = 4 ℃
+ 12.5 mM Ca2+
T = 4 ℃
+ 37.5 mM Ca2+
T = 4 ℃
a
b
c
d
e
f
g
h
i
j
k
l
m
n
o
p
q
r

319

320

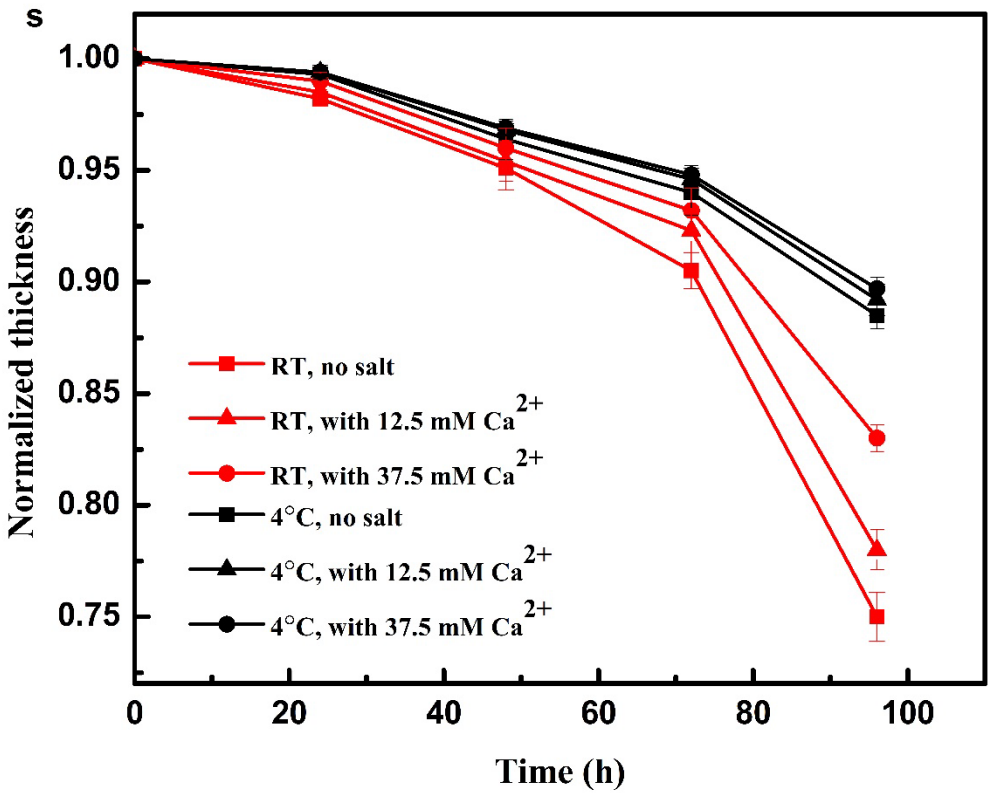

Figure 5. As-printed 40-layer scaffold using GB/XG mixed gels (a-c) with no salt addition (d-f) with 12.5 mM Ca^{2+} and (g-i) with 37.5 mM Ca^{2+} addition after printing 0, 24 and 96 h stored at room temperature (22 ± 1°C). As-printed 40-layer scaffold using GB/XG mixed gels (j-l) with no salt addition (m-o) with 12.5 mM Ca^{2+} addition and with 37.5 mM Ca^{2+} addition (p-r) after printing 0, 24 and 96 h at stored at 4 °C. (s) Normalized thickness of the scaffolds fabricated using GB/XG food ink with 0, 12.5 mM and 37.5 mM Ca^{2+} addition stored at room temperature and 4 °C over a period of 96 h. Scale bars are 5 mm.

The dimensional stability of 3D-printed structures was investigated as it is essential for food storage. A 4 day duration was chosen as a goal for ready-to eat food storage. **Figures 5a-r** presents the structure images showing the effect of Ca^{2+} addition and storage temperature after printing on the dimension of as-printed 3D scaffolds with respect to time. In general, adding Ca^{2+} or decreasing temperature improves the dimensional stability. Printed scaffold with sharper outline can be obtained for the GB/XG ink with added Ca^{2+} (**Figure 5d and 5g**) compared to the salt-free ink (**Figure 5a**). Besides, shape retention improves when increasing Ca^{2+} concentration (**Figure 5d and 5g**). The same phenomena has been reported based on the gelation quality of calcium-

enhanced alginate gels (Dalheim, et al., 2019) and pectin gels (Vancauwenberghe, et al., 2017). As the shape fidelity after deposition is closely related to the yield stress, the apparent yield stress of different food inks was calculated based on the method by Bruneaux et al. (Bruneaux, et al., 2008), and the results are shown in **Figure S2**. The apparent yield stress of food inks increases with a linear concentration dependence on Ca^{2+} in the range of 0 to 62.5 mM, which explains the better shape retention after printing. The high apparent yield stress is probably due to the reinforced gel network with Ca^{2+} addition. The latter modifies the flow properties but also helps to induce gelation (Freitas, et al., 2013; Mohammed, et al., 2007; Patel, et al., 2020) and maintain the 3D structure during and after printing . On the other hand, lowering the storage temperature results in good shape retention ability of the 3D printed scaffolds (**Figure 5m-5r**). The increased *G*' at low temperature from the rheological results (**Figure 4**) can also justify the superior shape retention. Besides, low temperature slows down the solvent evaporation, hence a higher shape fidelity of the hydrogel is retained.

Figure 5s shows the dimensional stability of the as-printed scaffolds by monitoring the evolution of the relative thickness variation to quantify the structure slumping. All the samples retain at least 75 % of their initial thickness after 96 h, indicating a satisfactory shape stability with food ink using the GB/XG pair. Comparably, thickness reduction using the food ink with 12.5 mM and 37.5 mM Ca^{2+} is 3% and 8% slower than the one with salt-free ink. In addition, the thickness reduction for scaffolds with both GB/XG and GB/XG/Ca^{2+} food ink is quite similar at 4 °C, showing around 11% reduction after 96 h, indicating that the storage temperature effects dominate dimensional stability compared to the salt effect.

Overall, the dimensional stability agrees well with the fact that the rheological properties are enhanced when adding Ca^{2+} or decreasing temperature.

3.4 Compression testing for textural profile analysis (TPA)

TPA is one of the most common measurement method for describing the characteristics of gels (Tao, et al., 2021), which includes hardness, adhesiveness, cohesiveness, springiness and gumminess. These characteristics are strongly related with the sensory perception of food (Çakır, et al., 2012). Scaffolds with different infill percentage were first printed (**Figure 6**) and were then tested for TPA. The calculated textural parameters are shown in **Figure 7** (**Table S4** for more

details) in order to clarify the effect of infill percentage of 3D scaffolds, Ca^{2+} concentration in the GB/XG food ink and storage temperature of printed scaffolds on basic textural properties.

Hardness is related to the sensory perception of the first bite in the mouth, which is the most direct reaction mouthfeel (Chandra & Shamasundar, 2014). It is represented by the peak force of the first compression cycle. The effects of infill percentages, salt concentrations and storage temperature on the hardness of the samples are shown in **Figure 7a**. Increasing the infill percentage causes an increase in the hardness. Specifically, the samples with 96% infill percentage have a significant higher hardness value compared to the ones with lower infill percentage ($p < 0.05$). The scaffolds with 25% infill percentage collapsed easily upon compressing because of the small contact filament area with the probe and thus high pressure. One interesting point to mention here is that the infill percentage can be well controlled during the 3D food model design process, so it can meet any specific requirements in terms of food texture, highlighting the potential of 3D printing. A significant difference in hardness was also observed for the samples containing different Ca^{2+} concentration ($p < 0.05$). GB/XG food ink with 62.5 mM Ca^{2+} addition has the highest hardness value of 57.3 g. Regarding the effect of storage temperature, it has an inverse relationship with hardness. That is, a decrease in storage temperature leads to an increase in the hardness, which is probably due to the formed stiffer structure, as discussed above.

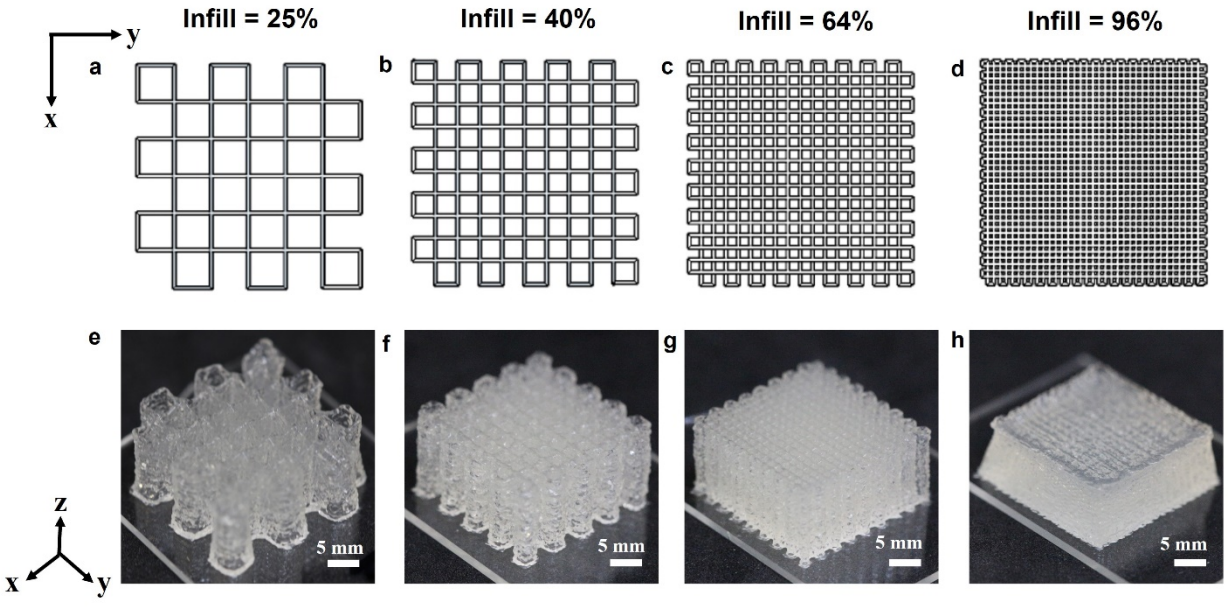

Figure 6. (a-d) Top-view models of scaffold with different infill percentage. (e-h) Representative images of 3D printed scaffold with different infill percentage using GB/XG with 37.5 mM Ca^{2+} food ink at room temperature right after printing. The printing times for scaffolds with different infill percentages were varying between 8 and 30 min.

When retracting the probe, a negative force arises from the attraction between the sample surface and the probe. Adhesiveness is defined as the negative area of force when the probe withdraws after the first compression. It can be interpreted as a sticky mouthfeel (Siamand, Deeth, & Al-Saadi, 2014). Appropriate adhesiveness benefits the taste and flavor releasing. However, too strong adhesiveness may cause the food sticking to the inner packaging, thus a structural damage when removing the packaging (Chandra, et al., 2014). The adhesiveness for samples with different infill percentages, salt concentrations and storage temperatures are shown in **Figure 7b**. The scaffold with the densest structure has a significant higher adhesiveness of 183 ± 3 g.s, because of the larger contact surface ($p < 0.05$). Adding Ca^{2+} to the ink also results in an increase of adhesiveness, with the sample containing 62.5 mM having a significant higher value ($p < 0.05$), which might be explained by the increased *G"* after Ca^{2+} addition. Similar observations for XG-based food gels have been reported before (Yang, Tsai, Jiang, & Hua, 2021). As for storage temperature, lower adhesiveness is observed at 4 ℃ because the structures containing GB become more elastic, as mentioned before.

The cohesiveness indicates the strength of internal bonds making up the body of food and the degree to which a food can be deformed before it breaks. It is defined as the ratio of the positive force area during the second compression to that of the first compression (Siamand, et al., 2014). Cohesiveness comparison of infill percentages, salt concentrations and storage temperatures effects are shown in **Figure 7c**. Samples with higher infill percentage shows stronger cohesiveness because of a relatively more stable structure against compression. The higher apparent yield stress for the food ink with higher Ca^{2+} provides better resistance against the deformation and thus benefits the cohesiveness of the printed scaffold. Moreover, food ink at low temperature demonstrates a higher gel strength, which translates into a larger tensile strength and higher cohesiveness of the printed scaffolds.

Gumminess is defined as the product of hardness and cohesiveness, which indicates the required energy to disintegrate food for swallowing (Nishinari & Fang, 2018). It is another important

textural characteristics, especially for semisolid food with a low degree of hardness and high degree of cohesiveness (Chandra, et al., 2014). In our case, gumminess exhibits a similar trend to hardness, regardless of the effects of infill percentage, salt concentration and storage temperature, as shown in **Figure 7d**. This indicates that the gumminess of printed samples is dominated by their hardness (Yang, et al., 2021).

Overall, food texture can be tuned by the rheological properties of the food ink, infill percentage during 3D printing and storage temperature. By carefully controlling the food ink properties and the designed form, it is possible to create group-specific food constructs according to their requirements. Food model designed with 100% infill are more popular in visual sight, while it is more acceptable in terms of mouthfeel with 25% infill (Mantihal, Prakash, & Bhandari, 2019). Some special groups of people such as dysphagic patients with swallowing difficulties are usually not able to consume food with high adhesiveness (Bychkov, Reshetnikova, Bychkova, Podgorbunskikh, & Koptev, 2021). 3D printing shows its ability control food properties for a large range of needs. For food applications, the 3D printed scaffolds using our food inks have a similar range of adhesiveness and cohesiveness as cheddar (Y. Zheng, Liu, & Mo, 2016), while their hardness and gumminess values can be referred to that of Jello™ (T. K. Kim, et al., 2020) and pudding (Park, Lee, Yoo, & Nam, 2020; J. Zheng, Wu, Dai, Kan, & Zhang, 2017). This shows the great potential to use the mixture of GB and XG to simulate the texture of soft food, well in agreement with a previously published work by Cohen et al.(Cohen, et al., 2009).

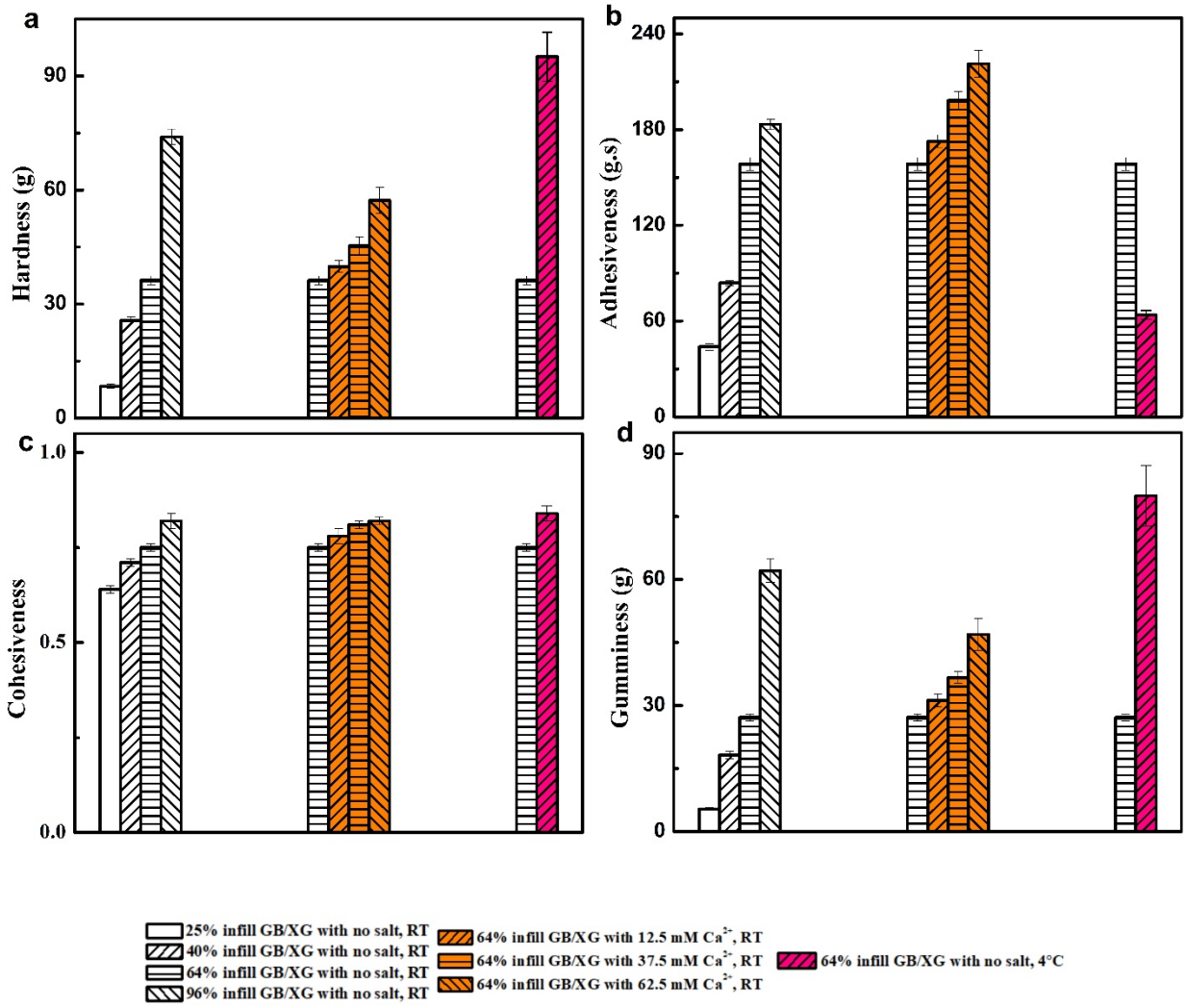

Figure 7. Ca^{2+} concentration, infill percentage and storage temperature effects on (a) hardness (b) adhesiveness (c) cohesiveness and (d) gumminess.

4. Conclusions

We successfully 3D printed food-grade scaffolds with ink composed of GB mixed with XG. The GB/XG ink exhibits a shear-thinning behavior, which allows the food ink to be easily extruded from the printer nozzle. GB is a key component as it endows the ink with improved rheological properties and the scaffold with better dimensional stability compared to that of XG alone. The addition of Ca^{2+} to GB/XG ink improves the printing results due to its bridging effect. Scaffolds exhibited the best structure and shape retention using food ink with the addition of 37.5 mM Ca^{2+}.

However, ink with 62.5 mM Ca^{2+} can cause irregular filaments and structure defects possibly because it causes over-gelation of the food ink. All printed scaffolds using GB/XG can retain more than 75% of their original thickness after 96 h of storage at room temperature, regardless of the presence of Ca^{2+}, exhibiting a high shape fidelity retention. Scaffolds with both GB/XG and GB/XG/Ca^{2+} food ink show the lowest thickness reduction - around 11% - after 96 h at 4 °C. Finally, the textural properties of the printed food scaffold can be modulated by adding Ca^{2+} to the ink, controlling the infill percentage through the 3D printing process and using different storage temperature after printing. This provides the possibility to use the 3D printing technique to shape group-specific food formulations according to different needs, such as those of elderly people or dysphagic patients.

Acknowledgements

This work is supported by the Natural Sciences and Engineering Research Council of Canada (NSERC). The authors acknowledge Mr. Ray Valli from CP Kelco U.S., Inc for providing the XG samples. The authors also thank China Scholarship Council (CSC) for providing a scholarship to C. Zhang.

References

Ansari, S., Rashid, M. A. I., Waghmare, P. R., & Nobes, D. S. (2020). Measurement of the flow behavior index of Newtonian and shear-thinning fluids via analysis of the flow velocity characteristics in a mini-channel. *SN Applied Sciences, 2*(11).

Bello, A. B., Kim, D., Kim, D., Park, H., & Lee, S. H. (2020). Engineering and Functionalization of Gelatin Biomaterials: From Cell Culture to Medical Applications. *Tissue Eng Part B Rev, 26*(2), 164-180.

Bertrand, M.-E., & Turgeon, S. L. (2007). Improved gelling properties of whey protein isolate by addition of xanthan gum. *Food Hydrocolloids, 21*(2), 159-166.

Bruneaux, J., Therriault, D., & Heuzey, M.-C. (2008). Micro-extrusion of organic inks for direct-write assembly. *Journal of Micromechanics and Microengineering, 18*(11).

Bychkov, A., Reshetnikova, P., Bychkova, E., Podgorbunskikh, E., & Koptev, V. (2021). The current state and future trends of space nutrition from a perspective of astronauts' physiology. *International Journal of Gastronomy and Food Science, 24*.

Çakır, E., Daubert, C. R., Drake, M. A., Vinyard, C. J., Essick, G., & Foegeding, E. A. (2012). The effect of microstructure on the sensory perception and textural characteristics of whey protein/κ-carrageenan mixed gels. *Food Hydrocolloids, 26*(1), 33-43.

Chandra, M. V., & Shamasundar, B. A. (2014). Texture Profile Analysis and Functional Properties of Gelatin from the Skin of Three Species of Fresh Water Fish. *International Journal of Food Properties, 18*(3), 572-584.

Chang, I., Im, J., Prasidhi, A. K., & Cho, G.-C. (2015). Effects of Xanthan gum biopolymer on soil strengthening. *Construction and Building Materials, 74*, 65-72.

Chen, J., Mu, T., Goffin, D., Blecker, C., Richard, G., Richel, A., & Haubruge, E. (2019). Application of soy protein isolate and hydrocolloids based mixtures as promising food material in 3D food printing. *Journal of Food Engineering, 261*, 76-86.

Cohen, D. L., Lipton, J. I., Cutler, M., Coulter, D., Vesco, A., & Lipson, H. (2009). Hydrocolloid Printing: A Novel Platform for Customized Food Production. In *Presentation at 20st annual international solid freeform fabrication symposium*. Austin, Texas.

Dalheim, M. O., Omtvedt, L. A., Bjorge, I. M., Akbarzadeh, A., Mano, J. F., Aachmann, F. L., & Strand, B. L. (2019). Mechanical Properties of Ca-Saturated Hydrogels with Functionalized Alginate. *Gels, 5*(2).

de Moura, M. R. V., & Moreno, R. B. Z. L. (2019). Concentration, Brine Salinity and Temperature effects on Xanthan Gum Solutions Rheology. *Applied Rheology, 29*(1), 69-79.

Drabek, J., Zatloukal, M., & Martyn, M. (2018). Effect of molecular weight on secondary Newtonian plateau at high shear rates for linear isotactic melt blown polypropylenes. *Journal of Non-Newtonian Fluid Mechanics, 251*, 107-118.

Du, J., Dai, H., Wang, H., Yu, Y., Zhu, H., Fu, Y., Ma, L., Peng, L., Li, L., Wang, Q., & Zhang, Y. (2021). Preparation of high thermal stability gelatin emulsion and its application in 3D printing. *Food Hydrocolloids, 113*.

Freitas, I. R., Cortez-Vega, W. R., Pizato, S., Prentice-Hernández, C., & Borges, C. D. (2013). Xanthan Gum as a Carrier of Preservative Agents and Calcium Chloride Applied on Fresh-Cut Apple. *Journal of Food Safety, 33*(3), 229-238.

Godoi, F. C., Prakash, S., & Bhandari, B. R. (2016). 3d printing technologies applied for food design: Status and prospects. *Journal of Food Engineering, 179*, 44-54.

Gross, B. C., Erkal, J. L., Lockwood, S. Y., Chen, C., & Spence, D. M. (2014). Evaluation of 3D printing and its potential impact on biotechnology and the chemical sciences. *Anal Chem, 86*(7), 3240-3253.

Guo, S. Z., Heuzey, M. C., & Therriault, D. (2014). Properties of polylactide inks for solvent-cast printing of three-dimensional freeform microstructures. *Langmuir, 30*(4), 1142-1150.

J.A. Carmona, N. C., P. Ramírez and J. Muñoz. (2017). Rheology and Structural Recovery Kinetics of an Advanced Performance Xanthan Gum with Industrial Application. In (Vol. 27): Applied Rheology.

Joly-Duhamel, C., Hellio, D., Ajdari, A., & Djabourov, M. (2002). All Gelatin Networks: 2. The Master Curve for Elasticity†. *Langmuir, 18*(19), 7158-7166.

Keerthana, K., Anukiruthika, T., Moses, J. A., & Anandharamakrishnan, C. (2020). Development of fiber-enriched 3D printed snacks from alternative foods: A study on button mushroom. *Journal of Food Engineering, 287*.

Kim, H. W., Bae, H., & Park, H. J. (2017). Classification of the printability of selected food for 3D printing: Development of an assessment method using hydrocolloids as reference material. *Journal of Food Engineering, 215*, 23-32.

Kim, T. K., Yong, H. I., Jang, H. W., Kim, Y. B., Sung, J. M., Kim, H. W., & Choi, Y. S. (2020). Effects of hydrocolloids on the quality characteristics of cold-cut duck meat jelly. *J Anim Sci Technol, 62*(4), 587-594.

Kumar, A., & Saini, C. S. (2021). Edible composite bi-layer coating based on whey protein isolate, xanthan gum and clove oil for prolonging shelf life of tomatoes. *Measurement: Food, 2*.

Lanaro, M., Forrestal, D. P., Scheurer, S., Slinger, D. J., Liao, S., Powell, S. K., & Woodruff, M. A. (2017). 3D printing complex chocolate objects: Platform design, optimization and evaluation. *Journal of Food Engineering, 215*, 13-22.

Le Tohic, C., O'Sullivan, J. J., Drapala, K. P., Chartrin, V., Chan, T., Morrison, A. P., Kerry, J. P., & Kelly, A. L. (2018). Effect of 3D printing on the structure and textural properties of processed cheese. *Journal of Food Engineering, 220*, 56-64.

Le, X. T., & Turgeon, S. L. (2013). Rheological and structural study of electrostatic cross-linked xanthan gum hydrogels induced by β-lactoglobulin. *Soft Matter, 9*(11).

Lille, M., Nurmela, A., Nordlund, E., Metsä-Kortelainen, S., & Sozer, N. (2018). Applicability of protein and fiber-rich food materials in extrusion-based 3D printing. *Journal of Food Engineering, 220*, 20-27.

Liu, Z., Zhang, M., Bhandari, B., & Yang, C. (2018). Impact of rheological properties of mashed potatoes on 3D printing. *Journal of Food Engineering, 220*, 76-82.

Mantihal, S., Prakash, S., & Bhandari, B. (2019). Texture-modified 3D printed dark chocolate: Sensory evaluation and consumer perception study. *J Texture Stud, 50*(5), 386-399.

McClements, D. J. (2006). Non-covalent interactions between proteins and polysaccharides. *Biotechnol Adv, 24*(6), 621-625.

Mohammed, Z. H., Haque, A., Richardson, R. K., & Morris, E. R. (2007). Promotion and inhibition of xanthan 'weak-gel' rheology by calcium ions. *Carbohydrate Polymers, 70*(1), 38-45.

Nishinari, K., & Fang, Y. (2018). Perception and measurement of food texture: Solid foods. *J Texture Stud, 49*(2), 160-201.

Ouyang, L., Yao, R., Zhao, Y., & Sun, W. (2016). Effect of bioink properties on printability and cell viability for 3D bioplotting of embryonic stem cells. *Biofabrication, 8*(3), 035020.

Park, J. W., Lee, S., Yoo, B., & Nam, K. (2020). Effects of texture properties of semi-solid food on the sensory test for pharyngeal swallowing effort in the older adults. *BMC Geriatr, 20*(1), 493.

Patel, J., Maji, B., Moorthy, N. S. H. N., & Maiti, S. (2020). Xanthan gum derivatives: review of synthesis, properties and diverse applications. *RSC Advances, 10*(45), 27103-27136.

Pelletier, E., Viebke, C., Meadows, J., & Williams, P. A. (2001). A rheological study of the order-disorder conformational transition of xanthan gum. *Biopolymers, 59*(5), 339-346.

Rao, M. A. (2014). Rheological Behavior of Processed Fluid and Semisolid Foods. In *Rheology of Fluid, Semisolid, and Solid Foods* (pp. 231-329).

Ross, A. C., Manson, J. E., Abrams, S. A., Aloia, J. F., Brannon, P. M., Clinton, S. K., Durazo-Arvizu, R. A., Gallagher, J. C., Gallo, R. L., Jones, G., Kovacs, C. S., Mayne, S. T., Rosen, C. J., & Shapses, S. A.

564 (2011). The 2011 report on dietary reference intakes for calcium and vitamin D from the Institute
565 of Medicine: what clinicians need to know. *J Clin Endocrinol Metab, 96*(1), 53-58.
566 Salehi, F. (2020). Edible Coating of Fruits and Vegetables Using Natural Gums: A Review. *International*
567 *Journal of Fruit Science, 20*(sup2), S570-S589.
568 Siamand, R., Deeth, H. C., & Al-Saadi, J. M. S. (2014). Textural and sensory properties of a calcium-induced
569 milk gel. *Journal of Food Engineering, 139*, 10-12.
570 Song, K.-W., Kim, Y.-S., & Chang, G.-S. (2006). Rheology of concentrated xanthan gum solutions: Steady
571 shear flow behavior. *Fibers and Polymers, 7*(2), 129-138.
572 Sun, J., Peng, Z., Zhou, W., Fuh, J. Y. H., Hong, G. S., & Chiu, A. (2015). A Review on 3D Printing for
573 Customized Food Fabrication. *Procedia Manufacturing, 1*, 308-319.
574 Sun, J., Zhou, W., Huang, D., Fuh, J. Y. H., & Hong, G. S. (2015). An Overview of 3D Printing Technologies
575 for Food Fabrication. *Food and Bioprocess Technology, 8*(8), 1605-1615.
576 Sun, J., Zhou, W., Yan, L., Huang, D., & Lin, L.-y. (2018). Extrusion-based food printing for digitalized food
577 design and nutrition control. *Journal of Food Engineering, 220*, 1-11.
578 Tao, H., Wang, B., Wen, H., Cui, B., Zhang, Z., Kong, X., & Wang, Y. (2021). Improvement of the textural
579 characteristics of curdlan gel by the formation of hydrogen bonds with erythritol. *Food*
580 *Hydrocolloids, 117*.
581 Tolstoguzov, V. B. (1995). Some physico-chemical aspects of protein processing in foods. Multicomponent
582 gels. *Food Hydrocolloids, 9*(4), 317-332.
583 Vancauwenberghe, V., Katalagarianakis, L., Wang, Z., Meerts, M., Hertog, M., Verboven, P., Moldenaers,
584 P., Hendrickx, M. E., Lammertyn, J., & Nicolaï, B. (2017). Pectin based food-ink formulations for 3-
585 D printing of customizable porous food simulants. *Innovative Food Science & Emerging*
586 *Technologies, 42*, 138-150.
587 Wang, C.-S., Natale, G., Virgilio, N., & Heuzey, M.-C. (2016). Synergistic gelation of gelatin B with xanthan
588 gum. *Food Hydrocolloids, 60*, 374-383.
589 Wang, C.-S., Virgilio, N., Carreau, P. J., & Heuzey, M.-C. (2021). Understanding the Effect of Conformational
590 Rigidity on Rheological Behavior and Formation of Polysaccharide-Based Hybrid Hydrogels.
591 *Biomacromolecules, 22*(9), 4016-4026.
592 Wang, C.-S., Virgilio, N., Wood-Adams, P. M., & Heuzey, M.-C. (2018). A gelation mechanism for
593 gelatin/polysaccharide aqueous mixtures. *Food Hydrocolloids, 79*, 462-472.
594 Wang, C. S., Virgilio, N., Wood-Adams, P., & Heuzey, M. C. (2017). A mechanism for the synergistic gelation
595 properties of gelatin B and xanthan gum aqueous mixtures. *Carbohydr Polym, 175*, 484-492.
596 Wang, L., Xiang, D., Li, C., Zhang, W., & Bai, X. (2021). Effects of lyophilization and low-temperature
597 treatment on the properties and conformation of xanthan gum. *Food Hydrocolloids, 112*.
598 Wang, L., Zhang, M., Bhandari, B., & Yang, C. (2018). Investigation on fish surimi gel as promising food
599 material for 3D printing. *Journal of Food Engineering, 220*, 101-108.
600 Wang, X.-Y., Wang, C.-S., & Heuzey, M.-C. (2015). Complexation of chitosan and gelatin: From soluble
601 complexes to colloidal gel. *International Journal of Polymeric Materials and Polymeric*
602 *Biomaterials, 65*(2), 96-104.
603 Warner, E. L., Norton, I. T., & Mills, T. B. (2019). Comparing the viscoelastic properties of gelatin and
604 different concentrations of kappa-carrageenan mixtures for additive manufacturing applications.
605 *Journal of Food Engineering, 246*, 58-66.
606 Wegrzyn, T. F., Golding, M., & Archer, R. H. (2012). Food Layered Manufacture: A new process for
607 constructing solid foods. *Trends in Food Science & Technology, 27*(2), 66-72.
608 Williams, P. A., & Phillips, G. O. (2003). The use of hydrocolloids to improve food texture. In *Texture in*
609 *Food* (pp. 251-274).

610 Yang, H., Tsai, C. C., Jiang, J. S., & Hua, C. C. (2021). Rheological and Textural Properties of Apple Pectin-
611 Based Composite Formula with Xanthan Gum Modification for Preparation of Thickened Matrices
612 with Dysphagia-Friendly Potential. *Polymers (Basel), 13*(6).
613 Zatz, J. L., & Knapp, S. (1984). Viscosity of xanthan gum solutions at low shear rates. *J Pharm Sci, 73*(4),
614 468-471.
615 Zeeb, B., Thongkaew, C., & Weiss, J. (2014). Theoretical and practical considerations in electrostatic
616 depositioning of charged polymers. *Journal of Applied Polymer Science, 131*(7), n/a-n/a.
617 Zhang, H. J., Wang, L., Wang, X., Han, Q., & You, X. (2020). Developing super tough gelatin-based hydrogels
618 by incorporating linear poly(methacrylic acid) to facilitate sacrificial hydrogen bonding. *Soft*
619 *Matter, 16*(20), 4723-4727.
620 Zheng, J., Wu, J., Dai, Y., Kan, J., & Zhang, F. (2017). Influence of bamboo shoot dietary fiber on the
621 rheological and textural properties of milk pudding. *Lwt, 84*, 364-369.
622 Zheng, Y., Liu, Z., & Mo, B. (2016). Texture Profile Analysis of Sliced Cheese in relation to Chemical
623 Composition and Storage Temperature. *Journal of Chemistry, 2016*, 1-10.

624